ISSN 1674-1056
http://cpb.iphy.ac.cn
http://iopscience.iop.org/cpb
中国物理 B
Chinese Physics
中国物理
Chinese Physics B

Complex alloying effect on thermoelectric transport properties of $Cu_2Ge(Se_{1-x}Te_x)_3$

Ruifeng Wang(王瑞峰), Lu Dai(戴璐), Yanci Yan(闫艳慈), Kunling Peng(彭坤岭), Xu Lu(卢旭), Xiaoyuan Zhou(周小元), Guoyu Wang(王国玉)
Citation: Chin. Phys. B . 2018, 27(6): 067201. **doi:** 10.1088/1674-1056/27/6/067201

Journal homepage: http://cpb.iphy.ac.cn; http://iopscience.iop.org/cpb

What follows is a list of articles you may be interested in

Thermoelectric properties of lower concentration K-doped $Ca_3Co_4O_9$ ceramics

Ya-Nan Li(李亚男), Ping Wu(吴平), Shi-Ping Zhang(张师平), Sen Chen(陈森), Dan Yan(闫丹), Jin-GuangYang(杨金光), Li Wang(王立), Xiu-Lan Huai(淮秀兰)
Chin. Phys. B . 2018, 27(5): 057201. **doi:** 10.1088/1674-1056/27/5/057201

Se substitution and micro-nano-scale porosity enhancing thermoelectric Cu_2Te

Xiaoman Shi(史晓曼), Guoyu Wang(王国玉), Ruifeng Wang(王瑞峰), Xiaoyuan Zhou(周小元), Jingtao Xu(徐静涛), Jun Tang(唐军), Ran Ang(昂然)
Chin. Phys. B . 2018, 27(4): 047204. **doi:** 10.1088/1674-1056/27/4/047204

Effect of Nb doping on microstructures and thermoelectric properties of $SrTiO_3$ ceramics

Da-Quan Liu(刘达权), Yu-Wei Zhang(张玉伟), Hui-Jun Kang(康慧君), Jin-Ling Li(李金玲), Xiong Yang(杨雄), Tong-Min Wang(王同敏)
Chin. Phys. B . 2018, 27(4): 047205. **doi:** 10.1088/1674-1056/27/4/047205

An overview of thermoelectric films: Fabrication techniques, classification, and regulation methods

Jing-jing Feng(冯静静), Wei Zhu(祝薇), Yuan Deng(邓元)
Chin. Phys. B . 2018, 27(4): 047210. **doi:** 10.1088/1674-1056/27/4/047210

Enhanced thermoelectric performance in p-type Mg_3Sb_2 via lithium doping

Hao Wang(王浩), Jin Chen(陈进), Tianqi Lu(陆天奇), Kunjie Zhu(朱坤杰), Shan Li(李珊), Jun Liu(刘军), Huaizhou Zhao(赵怀周)
Chin. Phys. B . 2018, 27(4): 047212. **doi:** 10.1088/1674-1056/27/4/047212

Complex alloying effect on thermoelectric transport properties of $Cu_2Ge(Se_{1-x}Te_x)_3$*

Ruifeng Wang(王瑞峰)[1,3], Lu Dai(戴璐)[1,3], Yanci Yan(闫艳慈)[1,2], Kunling Peng(彭坤岭)[1,2], Xu Lu(卢旭)[2], Xiaoyuan Zhou(周小元)[2], and Guoyu Wang(王国玉)[1,3,†]

[1] *Chongqing Institute of Green and Intelligent Technology, Chinese Academy of Sciences, Chongqing* 400714, *China*
[2] *College of Physics, Chongqing University, Chongqing* 401331, *China*
[3] *School of Physical Sciences, University of Chinese Academy of Sciences, Beijing* 100049, *China*

(Received 5 March 2018; revised manuscript received 3 April 2018; published online 30 May 2018)

To enhance the thermoelectric performance of Cu_2GeSe_3, a series of Te-alloyed samples $Cu_2Ge(Se_{1-x}Te_x)_3$ are synthesized and investigated in this work. It is found that the lattice thermal conductivity is reduced drastically for $x = 0.1$ sample, which may be attributed to the point defects introduced by alloying. However, for samples with $x \geq 0.2$, the lattice thermal conductivity increases with increasing x, which is related to a less distorted structure. The structure evolution, together with the change in carrier concentration, also leads to a systemically change in electrical properties. Finally, a zT of 0.55@750 K is obtained for the sample with $x = 0.3$, about 62% higher than that for the pristine sample.

Keywords: thermoelectric, Cu_2GeSe_3, alloying, distorted structure

PACS: 72.15.Jf, 61.66.Dk, 72.20.Pa, 66.70.Df **DOI:** 10.1088/1674-1056/27/6/067201

1. Introduction

As one of the possible solutions for the energy crisis and the environmental pollution, eco-friendly thermoelectric (TE) materials have intensively attracted worldwide attention in recent years due to its ability to directly convert heat into electricity and *vice versa*.[1–4] The performance of a TE material highly depends on its dimensionless TE figure of merit $zT = S^2\sigma T/\kappa$, where S is the Seebeck coefficient, σ the electrical conductivity, T the absolute temperature, and κ the total thermal conductivity. $S^2\sigma$, which is also known as the power factor (PF), is used to evaluate the electrical properties of a TE material. The total thermal conductivity κ can be divided into two parts: the lattice thermal conductivity κ_l and the electronic thermal conductivity κ_e. Great efforts have been paid for obtaining high zT materials which require both high PF and low thermal conductivity. Two general strategies have been proposed: enhancing electrical performance via the carrier concentration optimization sometimes assisted by band structure engineering,[5,6] and reducing lattice thermal conductivity by alloying[7] or nanostructuring.[8–10] Also, based on the phonon–glass electron–crystal (PGEC) concept,[11–13] many new TE materials have been discovered in the last two decades.

Cu-based chalcopyrite compounds with diamond-like structure have been widely reported recently[14–17] due to their high zTs, such as 1.18@850 K for $CuInTe_2$,[18] 1.4@950 K for $CuGaTe_2$,[19] and 0.91@860 K for $Cu_{2.1}Zn_{0.9}SnSe_4$.[20] Ternary Cu_2IVSe_3 (IV = Ge, Sn) is also a typical representative for Cu-based TE materials with diamond-like structure. Shi *et al.* reported that a high zT value of 1.14@850 K in $Cu_2Sn_{0.9}In_{0.1}Se_3$ was achieved,[21] associated with a relatively low thermal conductivity of around 1.0 $W\cdot m^{-1}\cdot K^{-1}$ at 850 K. By *ab initio* calculations, it was identified that Cu–Se network is responsible for the charge carriers transportation, while Sn atoms rarely make contribution to electrical transport but act as phonon scattering centers in the framework. Since Cu_2GeSe_3 has the same structure, similar band structure[22] and phonon spectrum[23] with Cu_2SnSe_3, the similar transport mechanism is expected in Cu_2GeSe_3. As a promising candidate for p-type TE material with a direct band gap (E_g = 0.78 eV),[24] the low thermal conductivity of Cu_2GeSe_3 was studied from both theoretical and experimental aspects. Cho *et al.* reported the occurrence of a large lattice anharmonicity (indicated by a high value of Grüneisen parameter) in Cu_2GeSe_3, and a high zT value of 0.5@750 K for Ga-doped samples.[25] Shao *et al.* investigated the phonon transport properties of Cu_2GeSe_3 by *ab initio* calculations, and argued that the weak covalent Cu-Se bonding rather than the strong lattice anharmonicity should be the origin of the low lattice thermal conductivity.[23] As the Cu_2SnSe_3 and Cu_2GeSe_3 have similarly low lattice thermal conductivity, comparable zT values are expected. However, a huge difference on the reported TE performance[25–29] exists between Cu_2SnSe_3 and Cu_2GeSe_3: Li *el al.* reported a record high zT of 1.42@823 K for $Cu_{1.85}Ag_{0.15}Sn_{0.9}In_{0.1}Se_3$,[30] whereas the highest zT is 0.65@758 K for $Cu_{1.95}GeSe_3$ re-

*Project supported by the National Natural Science Foundation of China (Grant Nos. 51672270, 11674040, and 11404044), the Key Research Program of Frontier Sciences, Chinese Academy of Sciences (Grant No. QYZDB-SSW-SLH016), and the Project for Fundamental and Frontier Research in Chongqing City (Grant No. CSTC2015JCYJBX0026).

†Corresponding author. E-mail: guoyuw@cigit.ac.cn

© 2018 Chinese Physical Society and IOP Publishing Ltd

ported by Huang *el al.*[27] The unexpected results motivate us to explore the possibility to enhance the TE performance of Cu_2GeSe_3.

In this work, Te is selected as alloying elements on Se sites for further reducing the lattice thermal conductivity of Cu_2GeSe_3 via alloying effect to promote TE performance. A series of $Cu_2Ge(Se_{1-x}Te_x)_3$ ($x = 0$, 0.1, 0.2, 0.3, 0.4) compounds are prepared and investigated. The results show that the lattice thermal conductivity for $x = 0.1$ is reduced by $\sim 35\%$ at 773 K compared to the pristine sample due to the alloying effect. A less distorted structure induced by increasing Te content impedes further reduction in lattice thermal conductivity for $x \geq 0.2$ samples. The carrier concentration also undergoes modulation by the change in defect concentration to some extent. Ultimately, a zT of 0.55@750 K is obtained for the $x = 0.3$ sample, approximately 62% higher than that of the pristine sample.

2. Experiment

$Cu_2Ge(Se_{1-x}Te_x)_3$ ($x = 0$, 0.1, 0.2, 0.3, 0.4) samples were synthesized by directly melting the stoichiometric amount of elements Cu (99.999%), Ge (99.999%), Se (99.999%), and Te (99.999%). The materials were first weighed in the glove box, put into fused silica tubes, sealed under high vacuum and heated up to 1173 K for 3 h, kept at that temperature for 12 h, and then furnace-cooled to room temperature. The obtained ingots were subsequently ground into powders, loaded into graphite die and sintered under dynamic vacuum with the uniaxial pressure of 45 MPa with a spark plasma sintering (SPS) system for densification. The highest temperature for SPS processing is 823 K and the holding period is 5 min. The relative density of the samples is measured by the Archimedes method and all the bulk samples show a density higher than 96% of the theoretical value.

Powder x-ray diffraction (XRD) patterns were collected using a PANalytical X'Pert apparatus with Cu–Kα radiation for the structure and phase analysis. Field emission scanning electron microscopy (JSM-7800 F, JEOL) was used for morphology and microstructure inspection. High-temperature electrical conductivity and Seebeck coefficient were measured by a commercial apparatus (LSR-3, Linseis, Germany) under a static helium atmosphere on the rectangular samples with the dimension of 2 mm×2 mm×8 mm. Thermal conductivity was calculated by the formula $\kappa = C_p \times D \times \rho$, where thermal diffusivity (D) was obtained by a laser flash diffusivity instrument (LFA 457, Netzsch, Germany) on the disk samples with a thickness of about 1.2 mm and a diameter of 10 mm. Specific heat (C_p) was determined by a differential scanning calorimetry (DSC 404, Netzsch, German), and density ρ is measured by the Archimedes method. The Hall coefficient (R_H) was obtained in a homemade Hall system with a magnetic field of ± 1 T. Hall mobility (μ_H) was calculated by the equation $\sigma = n_H \times q \times \mu_H$, where n_H is the Hall carrier concentration and q is the elementary charge. The measurement deviations on electrical conductivity, Seebeck coefficient, thermal conductivity were roughly 5%, 5%, and 7% respectively, and the total deviation on zT is estimated as 20%.

3. Results and discussion

Figure 1 shows the XRD patterns for $Cu_2Ge(Se_{1-x}Te_x)_3$ ($x = 0$, 0.1, 0.2, 0.3, 0.4) samples at room temperature. It is obvious that all the peaks shift to lower angle with increasing x, indicating expended lattice parameters since Te has a larger radius than Se.

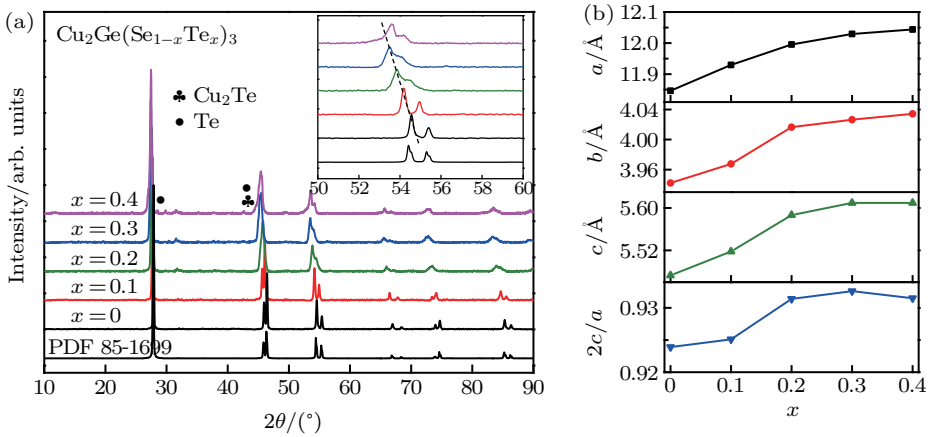


Fig. 1. (color online) (a) XRD patterns of $Cu_2Ge(Se_{1-x}Te_x)_3$ samples. The standard orthorhombic (PDF#85-1699) Cu_2GeSe_3 XRD patterns are also listed for comparison and the inset shows the enlargement of the patterns in the range of $50^\circ \leq 2\theta \leq 60^\circ$; (b) Alloying dependence of lattice parameters a, b, c, and the ratio of $2c/a$.

Another issue is that the 'double peaks', which is closely related to the ratio of lattice parameters $2c/a$ (in Cu_2GeSe_3, a is almost the same as $3b$, but a little different from $2c$), seems to merge into a 'single peak'. The enlargement of patterns in the range of $50^\circ \leq 2\theta \leq 60^\circ$ is shown in the inset of Fig. 1 as an example. The lattice parameters for all the samples are plotted in Fig. 1(b), together with the value for $2c/a$. The expansion of lattice parameters is confirmed, and the $2c/a$ shows

a tendency to approaching 1 with increasing Te content, which should be the reason why the 'double peaks' merged. Furthermore, a trace of impurity phases, Te and Cu_2Te, are observed in the sample with $x = 0.4$, indicating that the alloying limit of Te on Se sites is around $x = 0.3$.

Figure 2 shows the scanning electron microscopy (SEM) images of samples with $x = 0.1$ and $x = 0.4$. The grain size is on the order of μm, which confirms the advantage of SPS that it can suppress the growth of grain size during the sintering process. Another issue is that there are more pores in the sample with $x = 0.1$ than $x = 0.4$, which may be related to the higher melting point of Te than Se, since the sparking process may lead to local sublimation and sometimes create small pores in the sample.[27]

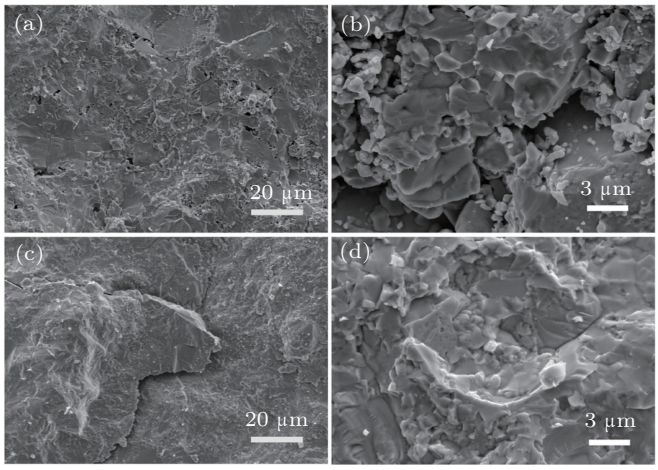


Fig. 2. SEM images for $Cu_2GeSe_{2.7}Te_{0.3}$ [(a) and (b)] and $Cu_2GeSe_{1.8}Te_{1.2}$ [(c) and (d)].

Figure 3(a) shows the temperature dependence of total thermal conductivity κ_{tot} for $Cu_2Ge(Se_{1-x}Te_x)_3$ ($x = 0$, 0.1, 0.2, 0.3, 0.4) samples. It is clear that the thermal conductivity drops with rising temperature, which is normal since the phonon–phonon scattering gets stronger at a higher temperature. The κ_{tot} of all the Te-alloyed samples is reduced compared with the pristine sample, and the minimum value of 0.54 $W{\cdot}m^{-1}{\cdot}K^{-1}$ at 773 K is obtained in the sample with $x = 0.1$, which is 37% lower than that of the pristine Cu_2GeSe_3. However for samples with $x \geq 0.2$, the κ_{tot} increases with increasing Te-alloying level. It is well known that the lattice thermal conductivity (κ_l) can be deducted by subtracting the electronic thermal conductivity κ_e from κ_{tot} via Wiedemann–Franz law: $\kappa_e = L\sigma T$, where the Lorenz constant L is obtained by the following equation

$$L = \left(\frac{k_B}{e}\right)^2 \left\{ \frac{(\lambda+7/2)F_{\lambda+5/2}(\eta)}{(\lambda+3/2)F_{\lambda+1/2}(\eta)} - \left[\frac{(\lambda+5/2)F_{\lambda+3/2}(\eta)}{(\lambda+3/2)F_{\lambda+1/2}(\eta)}\right]^2 \right\}. \quad (1)$$

The lattice thermal conductivity κ_l is shown in Fig. 3(b). It was reduced from 0.77 $W{\cdot}m^{-1}{\cdot}K^{-1}$ for the pristine sample to 0.50 $W{\cdot}m^{-1}{\cdot}K^{-1}$ for $x = 0.1$ at 773 K, which should be attributed to the stronger phonon scattering caused by the difference in atomic mass and radius between Te and Se atoms.

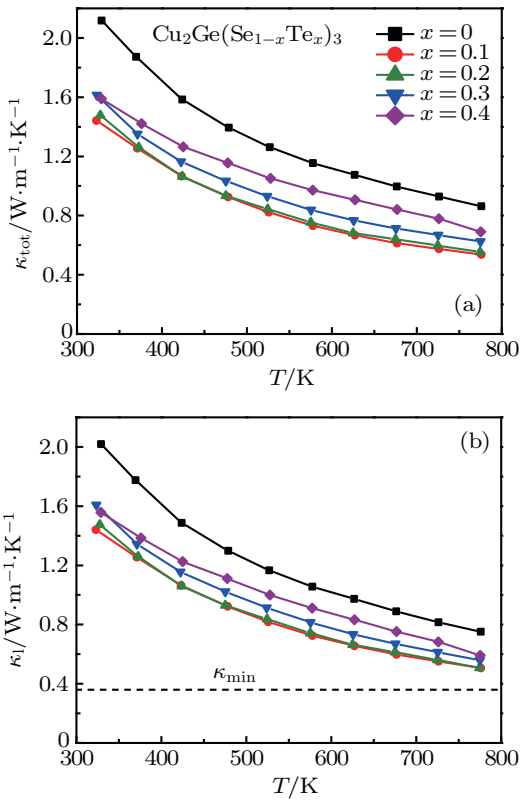


Fig. 3. (color online) Temperature dependence of (a) total thermal conductivity and (b) lattice thermal conductivity for $Cu_2Ge(Se_{1-x}Te_x)_3$ ($x = 0$, 0.1, 0.2, 0.3, 0.4). The dashed line in panel (b) is the minimum lattice thermal conductivity deduced from kinetic theory.

Shao *et al.*[23] studied the phonon spectra of Cu_2GeSe_3 by the first principle calculation and found that, the phonon density of states (DOS) at frequencies lower than 100 cm^{-1} are usually the dominating contribution for the heat transport and mainly derived from the Cu and Se vibrations. So the alloying of Te on Se sites will for sure disturb the phonon propagation. For samples with $x \geq 0.2$, κ_l shows the same tendency as κ_{tot} that it increases with increasing Te-alloying level. The approaching to a less distorted structure should be responsible for this abnormal phenomenon since distortion in lattice structure does not favor the propagation of phonons. The presence of two impurity phases Cu_2Te and Te, which has relatively higher lattice thermal conductivity, may also contribute to the high κ_l in the sample with $x = 0.4$. One may also consider the contribution from either the difference in sample density or in the microstructure, which does affect the lattice thermal conductivity. From Fig. 3 we did observe difference in microstructure in different samples, which may be one possible reason that leads to the difference in thermal conductivity; however for the sample relative density (D), as shown in Table 1, the biggest difference is within 3%, which is not high enough to lead such big difference in lattice thermal conductivity. From the kinetic theory, the minimum lattice thermal conductivity is

estimated by

$$\kappa_{\rm l} = \frac{1}{3} C_{\rm v} \nu_{\rm m} l, \tag{2}$$

where $C_{\rm v}$ is heat capacity (1.91×10^6 J·cm^{-3}·K^{-1}), $\nu_{\rm m}$ the mean sound velocity (2.4×10^3 m·s^{-1}), and l the mean free path of phonon (2.3 Å).[25] The value of $\kappa_{\rm lmin} = 0.36$ W·m^{-1}·K^{-1} is shown in Fig. 3(b) as a dashed line. It is clear that our experimental lattice thermal conductivity is still above the theoretical minimum value ($\kappa_{\rm lmin}$).

Figure 4 shows the electrical properties of $Cu_2Ge(Se_{1-x}Te_x)_3$ ($x = 0$, 0.1, 0.2, 0.3, 0.4). For pristine Cu_2GeSe_3, the electrical conductivity decreases and the Seebeck coefficient increases with increasing temperature, which is a typical behavior for degenerated semiconductor. With increasing Te content, the electrical conductivity first drops and then increases gradually and the Seebeck coefficient shows reversed tendency, as shown in Figs. 4(a) and 4(b). The carrier concentration for different samples at room temperature, deducted from Hall measurement, are shown in Table 1. The carrier concentration decreases from 9.8×10^{19} cm^{-3} in pristine sample to 5.0×10^{17} cm^{-3} in sample with $x = 0.1$, indicating that Te-alloying may decrease the defect concentration such as Cu_{Ge} for some unknown reasons. With further increasing Te amount, the carrier concentration gradually increases. Both the lower electronegativity of Te relative to Se, and the approaching to a less distorted lattice structure, will lead to a narrower band gap in the system. A narrower band gap has the tendency to make the defect level shallower, which leads to easier defect ionization and higher carrier concentration at a given temperature. So, the change of electrical conductivity and Seebeck coefficient with Te alloying amount can be easily understood according to the change of carrier density, since electrical conductivity and Seebeck coefficient is proportional and inversely proportional to carrier concentration, respectively. Figure 4(c) shows the temperature dependence of power factor (PF) for all samples. All the Te-alloyed samples show a big decreased PF at room temperature compared to the pristine sample, since the carrier concentration is tuned away from the optimized value.[27] The room temperature PF decreased from 0.24 mW·m^{-1}·K^{-2} for the pristine sample to 0.02 mW·m^{-1}·K^{-2} for the sample with $x = 0.1$, together with more than two orders decreasing in carrier concentration. However at high temperature, with further increasing of Te amount or the approaching of carrier concentration to the optimized value, the PF slowly recovered and the values for sample with $x = 0.3$ and 0.4 even exceed that for pristine sample. In addition, the PF increased with increasing Te content for $x \leq 0.3$, and then slightly decreased for $x = 0.4$. Again it is close related to the relative position to the optimized carrier concentration, which is in between 0.9×10^{19} cm^{-3} (for $x = 0.3$) and 5.4×10^{19} cm^{-3} (for $x = 0.4$).

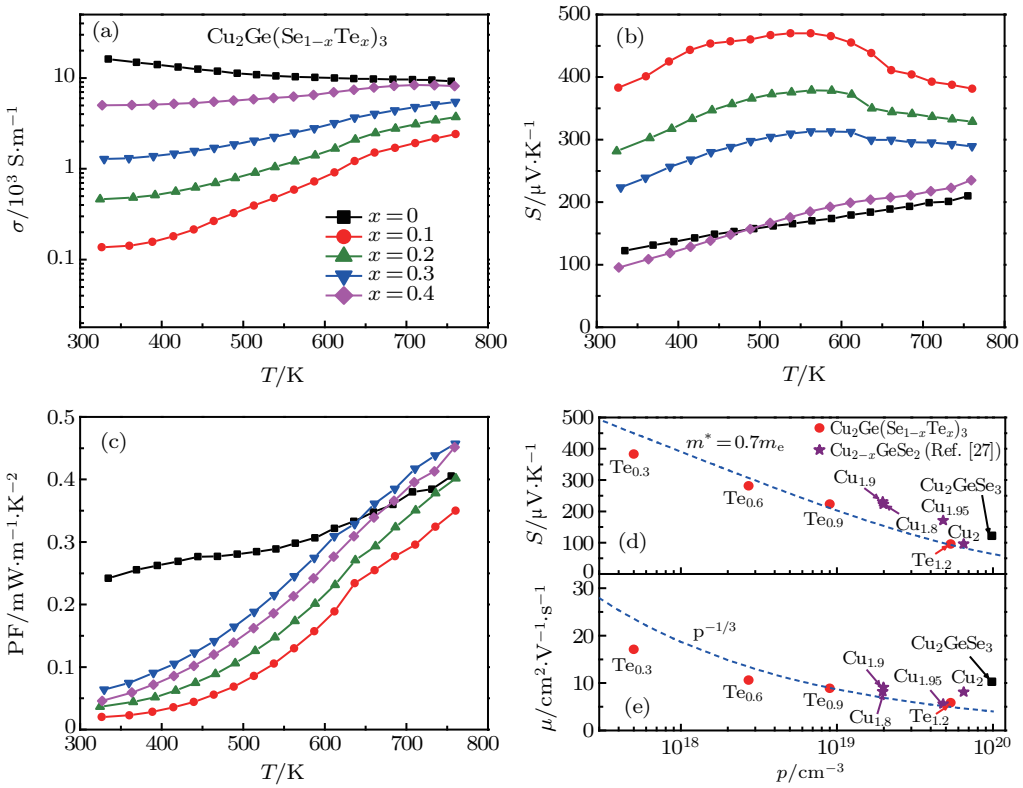


Fig. 4. (color online) Temperature dependence of (a) Seebeck coefficient, (b) electrical conductivity, and (c) power factor for $Cu_2Ge(Se_{1-x}Te_x)_3$ ($x = 0$, 0.1, 0.2, 0.3, 0.4) samples. Carrier density dependence of panel (d) Seebeck coefficient and (e) carrier mobility at 320 K. The dashed line in panel (d) is the Pisarenko curve simulated with $m^* = 0.7m_e$; The dashed line in panel (e) is a simulated curve for $\mu_{\rm H} \propto n_{\rm p}^{-1/3}$. Data from Ref. [24] are also plotted for reference.

Table 1. Parameters for $Cu_2Ge(Se_{1-x}Te_x)_3$ ($x = 0$, 0.1, 0.2, 0.3, 0.4) samples at room temperature.

Sample	$n_H/10^{19}$ cm^{-3}	$S/\mu V\cdot K^{-1}$	$\sigma/10^3$ S·m^{-1}	$\mu_H/cm^2\cdot V^{-1}\cdot s^{-1}$	D
Cu_2GeSe_3	9.8	122	16.7	10.5	98%
$Cu_2Ge(Se_{0.9}Te_{0.1})_3$	0.05	383	0.13	17.1	96%
$Cu_2Ge(Se_{0.8}Te_{0.2})_3$	0.27	281	0.46	10.6	97%
$Cu_2Ge(Se_{0.7}Te_{0.3})_3$	0.90	223	1.28	8.9	99%
$Cu_2Ge(Se_{0.6}Te_{0.4})_3$	5.4	96	5.02	5.8	97%

Figure 4(d) shows the relationship between Seebeck coefficient and carrier concentration at 320 K. The reported data in the Cu-deficient samples[27] is also plotted. According to the single parabolic band (SPB) model, the carrier concentration (n_p) and Seebeck coefficient (S) are described as

$$S = \frac{k_B}{e}\left(\frac{(5/2+\lambda)F_{3/2+\lambda}(\eta)}{(3/2+\lambda)F_{1/2+\lambda}(\eta)} - \eta\right), \tag{3}$$

and

$$n_p = 4\pi\left(\frac{2m^*k_BT}{h^2}\right)^{3/2} F_{1/2}(\eta), \tag{4}$$

where $\lambda = -1/2$ and η is the reduced chemical potential. The Fermi integrals are given by

$$F_j(\eta) = \int_0^\infty \frac{\xi^j \mathrm{d}\xi}{1+\exp(\xi-\eta)}, \tag{5}$$

where ξ is the reduced carrier energy and m^* is the density-of-states effective mass:

$$m^* = \frac{h^2}{2k_BT}\left[\frac{n_p}{4\pi F_{1/2(\xi)}}\right]^{2/3}. \tag{6}$$

Based on the SPB model, a dashed line for the Pisarenko curve with $m^* = 0.7m_e$ was drawn in Fig. 4(d). It can be seen that the data points at lower carrier concentration are below the dashed line but those at higher carrier concentration are above the dashed line. This phenomenon has been seen in many thermoelectric material systems, in which more bands contribute to the electrical transport when Fermi level is shifted downward. According to the formula $\sigma = n_H \times q \times \mu_H$, where n_H is the Hall carrier concentration, q the elementary charge, and μ_H the Hall mobility, the room temperature Hall mobility for all the samples were calculated and shown in Fig. 4(e). According to the typical electron-phonon mutual effect,[31–33] the relationship between mobility and carrier concentration can be expressed by $\mu_H \propto n_p^{-1/3}$ (see the dashed line in Fig. 4(e)). The mobility for pristine sample stands fairly above the dashed line but the mobility for sample with $x = 0.1$ sits well below the dashed line, indicating that the mobility suffers from the alloying of Te on Se sites. The disturbing of Cu–Se conducting network by Te-alloying should be responsible for this. However, the mobility starts to get closer to the dashed line with further increasing Te amount, suggesting the positive effect of less distorted structure on the carrier mobility.

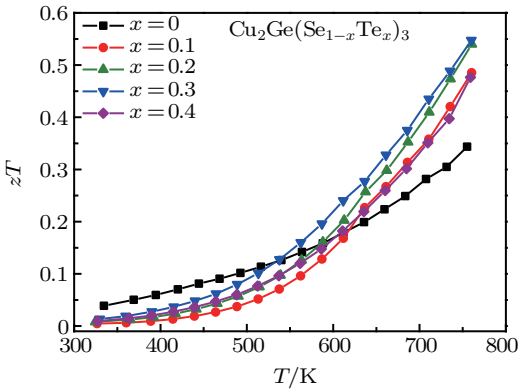


Fig. 5. (color online) The temperature-dependent zT values of $Cu_2Ge(Se_{1-x}Te_x)_3$ samples.

Temperature-dependence of zT is shown in Fig. 5. Though the PF is not very exciting for Te-alloyed samples, zT value is partially increased benefited from the decreased lattice thermal conductivity. The highest figure of merit zT is 0.55@750 K for the sample with $x = 0.2$ and 0.3, which is $\sim$62% higher than the pristine Cu_2GeSe_3. This value is not as high as the one reported by Huang *et al.*,[27] but still decent.

4. Conclusions

A series of $Cu_2Ge(Se_{1-x}Te_x)_3$ samples with diamond-like structure are prepared and investigated. Te alloying leads to the expansion of the lattice parameters, and also reduces the distortion in lattice structure. A small amount of Te-alloying on Se sites significantly decreases the lattice thermal conductivity *via* point defects. However more Te content leads to increased lattice thermal conductivity since the lattice structure is less distorted. The carrier mobility is suffered from Te alloying, which is the drawback of Te alloying. The electrical conductivity and Seebeck coefficient show clear dependence on Te alloying, which can be easily understood by the evolution of carrier concentration. Eventually, the Te alloying sample with $x = 0.3$ shows the maximum of $zT = 0.55$ at 750 K, which is enhanced by 62% than the pristine sample Cu_2GeSe_3.

References

[1] Snyder G J and Toberer E S 2008 *Nat. Mater.* **7** 105
[2] Bell L E 2008 *Science* **321** 1457
[3] Kraemer D, Jie Q, McEnaney K, Cao F, Liu W, Weinstein L A, Loomis J, Ren Z and Chen G 2016 *Nat. Energy* **1** 16153
[4] Yang J and Caillat T 2006 *MRS Bull.* **31** 224

[5] Pei Y, Shi X, LaLonde A, Wang H, Chen L and Snyder G J 2011 *Nature* **473** 66

[6] Zhao L D, Tan G, Hao S, He J, Pei Y, Chi H, Wang H, Gong S, Xu H, Dravid V P, Uher C, Snyder G J, Wolverton C and Kanatzidis M G 2016 *Science* **351** 141

[7] Skoug E J, Cain J D and Morelli D T 2010 *J. Alloys Compd.* **506** 18

[8] Hsu K F, Loo S, Guo F, Chen W, Dyck J S, Uher C, Hogan T, Polychroniadis E K and Kanatzidis M G 2004 *Science* **303** 818

[9] Biswas K, He J, Zhang Q, Wang G, Uher C, Dravid V P and Kanatzidis M G 2011 *Nat. Chem.* **3** 160

[10] Heremans J P, Dresselhaus M S, Bell L E and Morelli D T 2013 *Nat. Nanotechnol.* **8** 471

[11] Nolas G S, Slack G A, Chand J L and Schujman B 1998 *IEEE.* 294

[12] Nolas G S 1998 *Mrs Proc.* **545** 435

[13] Sales B C, Mandrus D and Williams R K 1996 *Science* **272** 1325

[14] Liu H, Shi X, Xu F, Zhang L, Zhang W, Chen L, Li Q, Uher C, Day T and Snyder G J 2012 *Nat. Mater.* **11** 422

[15] Chen Q, Wang G, Zhang A, Yang D, Yao W, Peng K, Yan Y, Sun X, Liu A, Wang G and Zhou X 2015 *J. Mater. Chem. C* **3** 12273

[16] Luo P, You L, Yang J, Xing J, Zhang J, Wang C, Zhao X, Luo J and Zhang W 2017 *Chin. Phys. B* **26** 097201

[17] Xue L, Xu B and Lin Y 2014 *Chin. Phys. B* **23** 037103

[18] Liu R, Xi L, Liu H, Shi X, Zhang W and Chen L 2012 *Chem. Commun.* **48** 3818

[19] Plirdpring T, Kurosaki K, Kosuga A, Day T, Firdosy S, Ravi V, Snyder G J, Harnwunggmoung A, Sugahara T, Ohishi Y, Muta H and Yamanaka S 2012 *Adv. Mater.* **24** 3622

[20] Liu M L, Chen I W, Huang F Q and Chen L D 2009 *Adv. Mater.* **21** 3808

[21] Shi X, Xi L, Fan J, Zhang W and Chen L 2010 *Chem. Mater.* **22** 6029

[22] Shao H, Zhang H, Peng B, Tan X, Liu G Q, Jiang J and Jiang H 2016 *Europhys. Lett.* **115** 26002

[23] Shao H, Tan X, Hu T, Liu G Q, Jiang J and Jiang H 2015 *Europhys. Lett.* **109** 47004

[24] Marcano G and Nieves L 2000 *J. Appl. Phys.* **87** 1284

[25] Cho J Y, Shi X, Salvador J R, Meisner G P, Yang J, Wang H, Wereszczak A A, Zhou X and Uher C 2011 *Phys. Rev. B* **84** 085207

[26] Zhao D, Ning J, Li S and Zuo M 2016 *J. Nanomater.* **2016** 5923975

[27] Huang T, Yan Y, Peng K, Tang X, Guo L, Wang R, Lu X, Zhou X and Wang G 2017 *J. Alloys Compd.* **723** 708

[28] Cho J Y, Shi X, Salvador J R, Yang J and Wang H 2010 *J. Appl. Phys.* **108** 073713

[29] Chetty R, Prem Kumar D S, Falmbigl M, Rogl P, You S W, Kim I H and Mallik R C 2014 *Intermetallics* **54** 1

[30] Li Y, Liu G, Cao T, Liu L, Li J, Chen K, Li L, Han Y and Zhou M 2016 *Adv. Funct. Mater.* **26** 6025

[31] Ong K P, Singh D J and Wu P 2011 *Phys. Rev. B* **83** 115110

[32] Wu W, Wu K, Ma Z and Sa R 2012 *Chem. Phys. Lett.* **537** 62

[33] Fan J, Liu H, Shi X, Bai S, Shi X and Chen L 2013 *Acta Mater.* **61** 4297